Meteorologische Zeitschrift, Vol. **27**, No. 4, 265–275 (published online August 2, 2018)

Modelling sound propagation from a wind turbine under various atmospheric conditions

Dietrich Heimann*

Deutsches Zentrum für Luft- und Raumfahrt, Institut für Physik der Atmosphäre, Weßling-Oberpfaffenhofen, Germany

(Manuscript received February 16, 2018; in revised form April 20, 2018; accepted May 1, 2018)

Abstract

Sound propagation from a wind turbine is investigated with the help of coupled atmospheric and acoustical simulation. Eight instants of time during nine diurnal cycles of idealized large-scale cases result in 72 meteorological situations for which the boundary-layer profiles of wind and temperature, the downstream wake flow of the rotor, and the sound propagation from the wind turbine into upwind and downwind direction were calculated. The resulting sound levels are evaluated relative to a non-refractive atmosphere to focus on the impact of meteorologically induced refraction. Within a range of 1 km from the turbine the sound levels vary stronger in upwind direction than in downwind direction, and the varying background wind speed at hub level causes a higher variability of the relative sound levels than the variations of the surface-layer stability. Surface-layer parameters turn out to be of only limited suitability for a meteorological classification of the wind-turbine noise impact.

Keywords: wind turbine, wake flow, sound propagation, diurnal cycle, numerical simulation

1 Introduction

Wind turbine noise is a major concern as the number of onshore wind converters increases and small turbines are substituted by higher and more powerful ones. Reliable noise predictions are therefore indispensable in the planning and approval process of new installations. Sound waves are generated by the interaction between the wind and the rotating blades (aerodynamic noise) or by other sources at the turbine and propagate through the atmospheric boundary layer (ABL). The vertical gradients of wind and temperature in the ABL cause upward and downward refraction, depending on the direction of propagation relative to the wind and the atmospheric stability. Turbulent eddies in the ABL lead to additional refraction and scattering according to whether the wave length is smaller or larger as the length scale of the turbules (Goedecke and Auvermann, 1997). In downwind direction, however, the ABL is additionally distorted by the wake of the turbine (Bingöl et al., 2010). In particular, the wind speed is reduced in a tube-like zone behind the rotor. The magnitude of the wind deficit and the length of this zone are influenced by the large-scale wind speed and the intensity of turbulent mixing. The latter depends on the static stability of the ABL (Gross, 2010; Hansen et al., 2012; Barlas et al., 2017a; Englberger and Dörnbrack, 2017). The wake leads to rather complex three-dimensional refraction conditions for downstream sound propagation.

The sound impact near the ground is a consequence of the sound emission characteristics at the source (source strength, frequency spectrum, directivity, e.g. Bowdler and Leventhall, 2012), and the propagation processes encountered between the elevated source positions and the near-ground receivers. These processes are air absorption, refraction, scattering, and reflection at the ground (e.g. Öhlund and Larsson, 2015). Meteorological variations influence the propagation processes, especially refraction. The source strength is also influenced by the atmospheric conditions and additionally by operational parameters (e.g. blade rotation speed, pitch and yaw). To be independent of the source strength this study focusses on the effect of refraction on the near-ground sound impact in the upwind and downwind domain of a wind turbine. Plane ground is assumed in these domains.

Results of coupled flow and sound propagation simulations have been published before, for instance by Heimann et al. (2011), Lee et al. (2016), Barlas et al. (2017a,b), Heimann et al. (2018), or Heimann and Englberger (accepted). In these studies only a few different situations were investigated. Now, coupled flow and sound propagation simulations are performed for nine different diurnal cycles of varying atmospheric stability under specific large-scale conditions. In total, 72 meteorological situations are investigated with respect to their refraction effects both in the upstream and downstream direction.

The models are briefly described in Section 2. The results are discussed in Section 3 with specific emphasis on the refraction effect on the near-ground sound impact. Finally, the results are discussed and conclusions are summarized in Section 4.

*Corresponding author: Dietrich Heimann, Deutsches Zentrum für Luft- und Raumfahrt, Institut für Physik der Atmosphäre Oberpfaffenhofen, 82234 Weßling, Germany, e-mail: dietrich.heimann@dlr.de

DOI 10.1127/metz/2018/0910

Gebrüder Borntraeger Science Publishers, Stuttgart, www.borntraeger-cramer.com

2 Numerical simulations

The study is based on coupled meteorological-acoustical numerical simulation. As a first step a one-dimensional boundary-layer model is used to generate diurnal cycles of the vertical profiles of wind, temperature and humidity for nine idealized large-scale cases. The large-scale horizontal pressure gradient is characterized by the geostrophic wind at ground level and at 500 m height, the mean temperature gradient, the dew point difference in the free atmosphere, and the roughness length of the ground. These parameters control the dynamic forcing, the surface heat budget and the kinematic boundary condition. The parameter setting of the nine cases is summarized in Table 1.

The one-dimensional boundary-layer model parameterizes the production and dissipation of turbulent kinetic energy according to Level 2.5 of Mellor and Yamada (1974). Near the ground flux-profile relationships after Paulson (1970) and Dyer (1974) are employed. The Coriolis force is included and causes turning wind direction in the Ekman layer. The short-wave and long-wave radiation transfer follows Pielke (1984), Chapter 8. A 5-layer soil model with standard parameters for grass-covered plane ground provides the fluxes of heat and moisture at the surface. In the atmosphere the one-dimensional model applies 30 levels with an increasing vertical spacing Δz ranging from $\Delta z = 2$ m near the ground to $\Delta z = 500$ m below the top at $z = 3000$ m. The initial conditions refer to adiabatic (neutral) stratification at 18 LT time (LT = local time), i.e. the transition from day to night. The model is integrated over 36 hours to generate a steady-state diurnal cycle for a cloud-less equinoctial situation at 50° northern latitude. After 12 hours, beginning with 06 LT, the profiles are stored in 3-hour intervals so that in total eight consecutive times of the day (06, 09, 12, 15, 18, 21, 00, 03 LT) are available per case for further evaluation.

In the next step a three-dimensional compressive Reynolds-averaged Navier-Stokes (RANS) model is applied to calculate the influence of the wind turbine on the boundary-layer flow over plane ground. The model is identical with "Model 2" in Heimann et al. (2011). The boundary-layer parameterization of the three-dimensional simulations corresponds to that of the one-dimensional precursory simulations. The model is initialized with the vertical wind and temperature profiles that resulted from the one-dimensional simulations for each of the nine large-scale cases and for all eight times of the day. In total 72 flow simulations are performed. 60 numerical levels are implemented with a vertical spacing of $\Delta z = 5$ m up to a height of $z = 300$ m. Horizontally the domain extends from $x = -250$ m (inflow boundary) to $x = +1250$ m (outflow boundary) and from $y = -152.5$ m to $y = +152.5$ m (lateral boundaries) with a numerical grid spacing of $\Delta x = \Delta y = 5$ m.

A three-blade wind turbine is located at $x_0 = y_0 = 0$. The hub of the rotor is situated at a height of $z_{hub} = 100$ m and the rotor diameter is set to $D = 2r = 100$ m

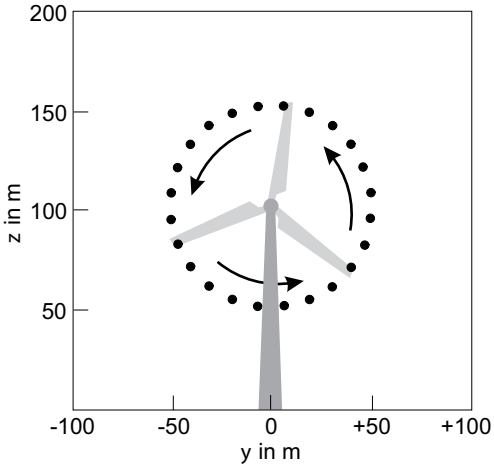

Figure 1: Geometry of the wind turbine as seen from the downwind side. The dots indicate the 24 sound emission points.

with r being the radius of the rotor. The force which the rotor exerts on the air flow is parameterized as described in Heimann et al. (2011). The three-dimensional flow model is integrated in time with a time step of $\Delta t = 0.007$ s until a steady-state mean flow field has been established. The model results comprise the three mean wind components $\bar{u}$, $\bar{v}$, and $\bar{w}$, the mean temperature $\bar{T}$, and the turbulent kinetic energy $\bar{E}$ at all $300 \times 61 \times 60$ grid points. Humidity is not considered in the three-dimensional simulations.

In a third and last step the results of the three-dimensional flow simulations are used as input for a three-dimensional ray-based sound propagation model. This Lagrangian sound particle model is described in Heimann and Gross (1999). The same model was already applied to the propagation of wind turbine noise by Heimann et al. (2011, 2018) and Heimann and Englberger (accepted). The rotor as the source of aerodynamic sound is modelled by 24 source points located 5 m off the blade tips, i.e. the circular source near the rotating blade tips is resolved in steps of 15 degrees (Fig. 1). The source is assumed to be incoherent so that the phase of the sound waves can be ignored. In contrast to Heimann et al. (2011) the source directivity is considered as described in Heimann et al. (2018). The frequency spectrum is applied for all 1/3-octave bands from 20 Hz to 16 kHz following Deutsche WindGuard (2015).

Each three-dimensional acoustical simulation is performed with 500,000 virtual sound particles, each of which carrying a specific amount of sound energy. The particles are released concurrently at the source points and travel along sound rays. The sound rays are straight in non-refractive homogeneous and calm air, but in the presence of wind and temperature gradients they are curved according to refraction (Pierce, 1981; Chapter 8). In addition to the mean flow, turbulence is considered by synthetically generated eddies of different size and strength which overlap each other and superimpose the mean flow. The size and power distribution of the

Table 1: Overview of the cases.

case	geostrophic wind speed horizontal large-scale pressure gradient		background temperature gradient	dewpoint difference	roughness length
	$z = 0$ m	$z = 500$ m		$z = 500$ m	
1	5 m/s 0.6042 Pa/km	5 m/s 0.6038 Pa/km	−4 K/500 m	6 K	0.1 m
2	10 m/s 1.2085 Pa/km	10 m/s 1.2081 Pa/km	−4 K/500 m	6 K	0.1 m
3	15 m/s 1.8127 Pa/km	15 m/s 1.8121 Pa/km	−4 K/500 m	6 K	0.1 m
4	7.5 m/s 0.9063 Pa/km	7.5 m/s 0.9061 Pa/km	−4 K/500 m	6 K	0.1 m
5	12.5 m/s 1.5106 Pa/km	12.5 m/s 1.5101 Pa/km	−4 K/500 m	6 K	0.1 m
6	2.5 m/s 0.3021 Pa/km	5 m/s 0.6040 Pa/km	−4 K/500 m	6 K	0.1 m
7	5 m/s 0.6256 Pa/km	5 m/s 0.6254 Pa/km	+5 K/500 m	15 K	0.1 m
8	5 m/s 0.6042 Pa/km	5 m/s 0.6040 Pa/km	−4 K/500 m	6 K	0.5 m
9	5 m/s 0.6042 Pa/km	5 m/s 0.6040 Pa/km	−4 K/500 m	6 K	0.01 m

vortices is chosen such that the bulk turbulent kinetic energy $\bar{E}$ and the −5/3 power law of the turbulent kinetic energy spectrum are locally fulfilled. The eddies modifiy the horizontal and vertical gradients of the wind speed and thus refraction. Turbulent temperature fluctuations are not considered as their effect on the effective sound speed is smaller than that of the wind fluctuations, at least for the wind speeds assumed here. The turbulence generator is fully described in Heimann and Blumrich (2004).

During propagation the sound particles lose energy due to air absorption according to ISO 9613-1. Sound particles that hit the ground are reflected (specular reflection) and lose energy according to the impedance ratio of ground and air. The impedance of the ground is parameterized after Delany and Bazley (1970) with a flow resistivity of $\sigma = 300\,\mathrm{kPa\,s\,m^{-2}}$. This value corresponds to dense, grass-covered ground. Two simulations are performed for each of the 72 situations: one in upwind direction and one in downwind direction. The acoustical domains comprise the volume confined by $-1000\,\mathrm{m} \le x \le 0$ (upwind domain), $0 \le x \le +1000\,\mathrm{m}$ (downwind domain), $-150\,\mathrm{m} \le y \le +150\,\mathrm{m}$, and $0 \le z \le +200\,\mathrm{m}$. The local sound level is determined in spherical receiver volumes of 5 m diameter where the specific sound energy of passing particles is added. The spacing of the receiver volume centres is $\Delta x = \Delta y = \Delta z = 5\,\mathrm{m}$ The starting directions of the particles are chosen so that all ground-based receiver volumes in the area $100\,\mathrm{m} \le |x| \le 1000\,\mathrm{m}$ and $-150\,\mathrm{m} \le y \le 150\,\mathrm{m}$ are crossed by sufficient particles to determine the local sound level with an acceptable accuracy of at least 0.1 dB. All sound levels discussed in the following refer to 'near ground', i.e. the lowest layer of receiver volumes with a nominal height of $z_R = 2.5\,\mathrm{m}$ above ground.

In addition to the 72 situations, two reference simulations were conducted for a homogeneous and windless, i.e. non-refractive atmosphere: one in upwind and one in downwind direction. The acoustical results are principally shown as A-weighted sound levels of the refractive situations L_A relative to that of a non-refractive atmosphere $L_{A,\mathrm{nr}}$, i.e. the sound-level difference $L_A - L_{A,\mathrm{nr}}$ is evaluated. L_A and $L_{A,\mathrm{nr}}$ correspond to a time-averaged sound level over a complete revolution of the rotor. Amplitude modulations (e.g. Larsson and Öhlund, 2014) are not considered. $L_A - L_{A,\mathrm{nr}}$ is independent of the source power and isolates the refraction effects due to the atmospheric gradients in the upwind and downwind domain. $L_A - L_{A,\mathrm{nr}}$ is referred to as 'relative sound level' in the following. Positive and negative values of the relative sound level imply enhancement and diminishment of the sound due to meteorologically induced refraction, respectively. As far as sound levels are averaged (spatially or within categories) logarithmic averaging $\bar{L} = 10\lg\left(\frac{1}{n}\sum_{i=1}^{n} 10^{L_i/10}\right)$ is applied.

3 Results

The results are presented and discussed in four steps: First, an overview of the meteorological variety of the

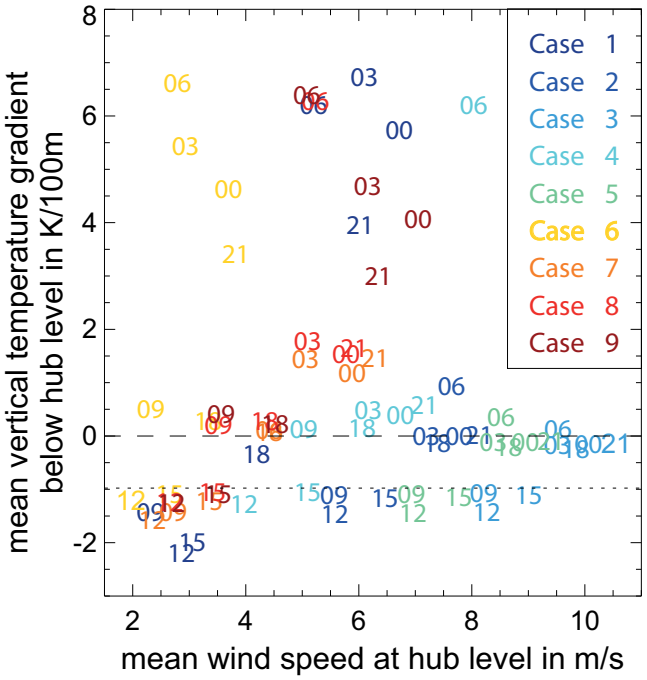

Figure 2: Distribution of the mean wind speed at hub level and the mean vertical temperature gradient below hub level of all 72 situations. The colours indicate the nine cases (cf. Table 1), the numbers refer to the eight times of the day (LT = local time). The dashed and dotted lines indicate isothermal and adiabatic temperature gradients, respectively.

nine diurnal cycles is visualized in Fig. 2. Second, vertical cross sections of the turbine-induced wind speed deficit and the acoustically relevant vertical gradient of the effective speed of sound are shown, by way of example, for two times of a day of one case (Figs. 3 and 4). Third, horizontal fields of the effect of refraction on the near-ground sound level are presented, again by way of example, for the morning situation of two cases in the upwind and downwind domain (Figs. 5 and 6). Finally, the acoustical results are summarized for the diurnal cycle of all nine cases, i.e. for all 72 situations (Figs. 7–10).

Fig. 2 shows the boundary-layer characteristics that resulted from the 1-dimensional model simulations at 00, 03,..., 21 LT for all nine large-scale conditions. The scatter diagram combines the mean wind speed at hub level $\bar{u}(z_{\mathrm{hub}})$ and the mean vertical temperature gradient γ in the layer between ground and hub level $\gamma = \left[\bar{T}(z_{\mathrm{hub}}) - \bar{T}(0)\right]/z_{\mathrm{hub}}$. Both parameters characterize the unmodified background meteorological environment of the wind turbine. The chosen situations cover a large range of wind speed and stability. Temperature inversions ($\gamma > 0$) appear during night and in the morning at 21, 00, 03 and 06 LT. Unstable stratification ($\gamma < -0.98\,\mathrm{K}/100\,\mathrm{m}$) mainly occurs at 12 and 15 LT. There are some situations with a combination of high wind speed $\bar{u}(z_{\mathrm{hub}})$ and strong inversion. In these cases the wind at hub level is influenced by a low-level jet that forms during night as a consequence of geostrophic-antitriptic imbalance. However, for strong winds $\bar{u}(z_{\mathrm{hub}}) > 8\,\mathrm{m/s}$ the stratification of the regarded situations is always near-neutral, i.e. $\gamma \approx -0.98\,\mathrm{K}/100\,\mathrm{m}$.

Downstream of the turbine the boundary-layer profiles are modified by the rotor which extracts kinetic energy from the flow. These modifications manifest themselves as a slight deceleration in front of the rotor and an elongated tube-like zone of rather strong wind speed reduction in the wake of the rotor. There are also weak accelerations below and above the rotor layer. Fig. 3 shows the turbine-induced wind speed deficit for Case 2, 00 and 12 LT. The strength and shape of the modifications depend on the static stability of the background boundary-layer. In the stable boundary layer (00 LT) the wind speed is strongly decelerated behind the rotor and the wake extends over a long distance. In the unstable situation (12 LT) the wake is much weaker and shorter. This behaviour is mainly due to the turbulence which is significantly stronger in unstable stratification. It causes mixing and a fast re-establishment of the background flow in the downstream domain of the turbine.

For the propagation of sound waves the gradients of the effective speed of sound are important as they determine refraction. The effective speed of sound $\bar{c}_{\mathrm{eff}} = \bar{c} + \bar{u}$ is composed of the adiabatic sound speed $\bar{c}$ relative to the air and the wind speed component $\bar{u}$ in the direction of propagation. The adiabatic sound speed is a function of the temperature

$$\bar{c} = \sqrt{\frac{c_p}{c_v} R_d \bar{T}} \tag{3.1}$$

where c_v and c_p are the specific heats of air for constant volume and constant pressure, respectively. R_d is the gas constant for dry air. Again for Case 2, 00 and 12 LT, Fig. 4 shows the vertical gradient of the effective speed of sound

$$\begin{aligned} \frac{\partial \bar{c}_{\mathrm{eff},-x}}{\partial z} &= \frac{\partial}{\partial z}(\bar{c} - \bar{u}) \quad \text{in upwind direction ;} \\ \frac{\partial \bar{c}_{\mathrm{eff},+x}}{\partial z} &= \frac{\partial}{\partial z}(\bar{c} + \bar{u}) \quad \text{in downwind direction} \end{aligned} \tag{3.2}$$

for propagation along the x-axis because it is the dominant direction of sound propagation in the upwind and downwind domain.

Fig. 4 shows the distribution of this gradient in the xz-plane for $y = 0$. In upwind direction the vertical gradient of $c_{\mathrm{eff},-x}$ is generally negative so that upward refraction prevails. In downwind direction the vertical gradient of $c_{\mathrm{eff},+x}$ is range-dependent with negative values in the rotor layer below the hub level and strong positive values near the ground and in the rotor layer above hub level. At greater distance from the turbine, positive values are dominant. In terms of refraction this means that sound is upward refracted in the lower half of the rotor layer ($z_{\mathrm{hub}} - r \le z \le z_{\mathrm{hub}}$) in the near-field of the turbine. In other layers and farther away from the turbine downward refraction prevails. Case 2, 12 LT, also shows that upward refraction can appear above the

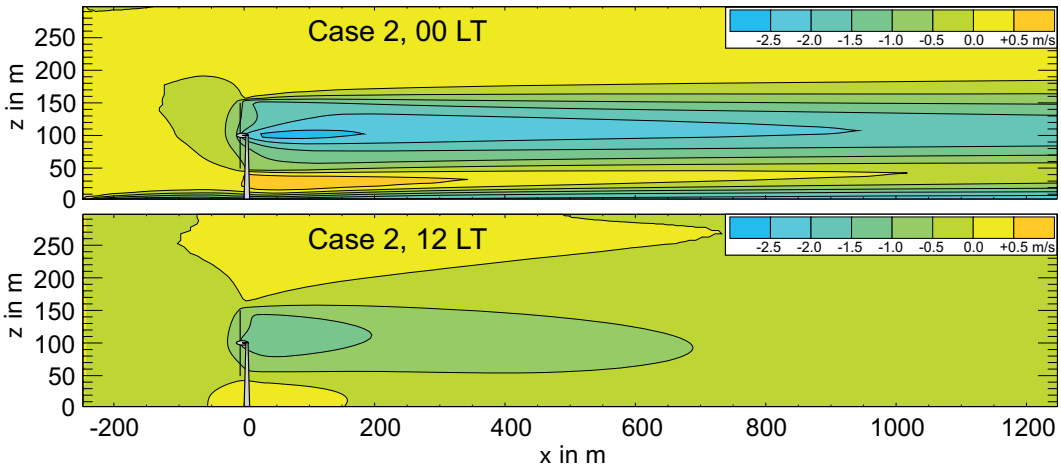

Figure 3: Vertical cross-section (x-z-plane along $y = 0$) of the deviation of the $\bar{u}$-component of the wind from the undisturbed inflow profile. Top: Case 2, 00 LT, bottom: Case 2, 12 LT.

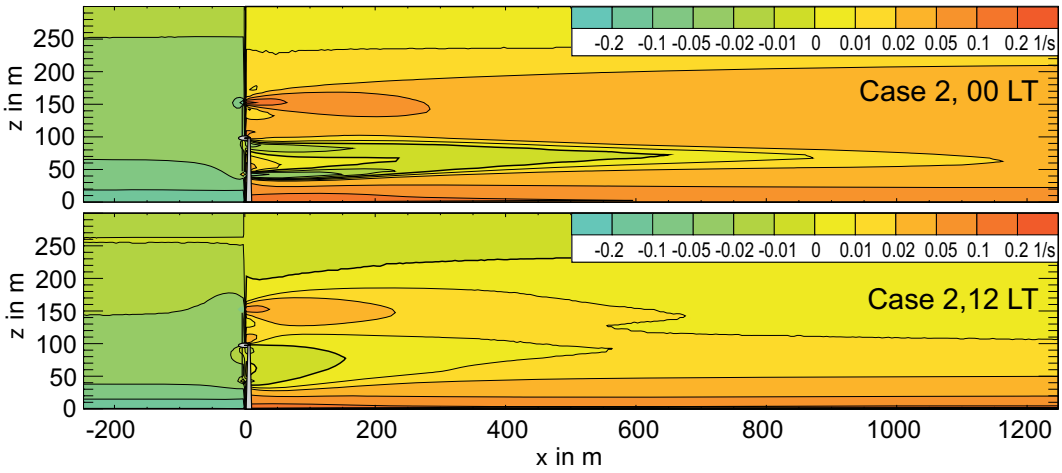

Figure 4: Vertical gradient of the effective speed of sound $\bar{c}_{\mathrm{eff},x}$ for propagation along the x-direction for Case 2. Top: 00 LT, bottom: 12 LT. Positive and negative values correspond to downward and upward refraction, respectively.

rotor layer when negative sound speed gradients in the unstable boundary-layer over-compensate the positive wind speed gradient.

The situations shown in Figs. 3 and 4 (Case 2, 00 and 12 LT) are to some degree typical, but they do not represent the full variety of all 72 situations. The consequences for the near-ground relative sound level $L_A - L_{A,\mathrm{nr}}$ are shown for two other situations, viz. Case 3, 06 LT, and Case 9, 06 LT. Figs. 5 and 6 illustrate that the same hour of the day, but for different meteorological background conditions can also lead to very different results. In the upwind domain (Fig. 5) upward refraction causes a partly shadowed zone in the far field ($x \leq -600\,\mathrm{m}$) with reduced sound levels in the strong-wind Case 3. On the contrary, the weak wind situation of Case 9 causes downward refraction with slightly increased sound levels. In this situation the positive vertical sound speed gradient in the morning inversion layer is not (over-) compensated by the vertical wind gradient. Both situations also differ in the downwind domain (Fig. 6). Here the strong wind situation of Case 3 leads to increased sound levels in the far field ($x \geq 700\,\mathrm{m}$), but only near the centreline ($|y| \approx 0$), that is beneath the wind speed deficit of the wake. The centred amplification also results from lateral refraction due to the horizontal wind speed gradients at the sides of the deficit region. In Case 9 refraction reduces the near-ground sound level rather strongly in the downwind domain (Fig. 6). In this case it is caused by the combination of three effects: (1) upward refraction by positive wind speed gradients in the lower part of the wind speed deficit region ($z_{\mathrm{hub}} - r \leq z \leq z_{\mathrm{hub}}$), (2) upward refraction by negative vertical temperature gradients above the ground-based inversion and (3) upward refraction by negative vertical wind speed gradients above the wind speed maximum of the low-level jet that has formed in the night of this case. The upward refraction prevents a larger part of the emitted sound energy from reaching the near-ground layer in the downwind domain.

The acoustical results of all 72 situations are presented in Fig. 7. It shows the horizontal profiles of the nearground relative sound levels $L_A - L_{A,\mathrm{nr}}$ in upwind

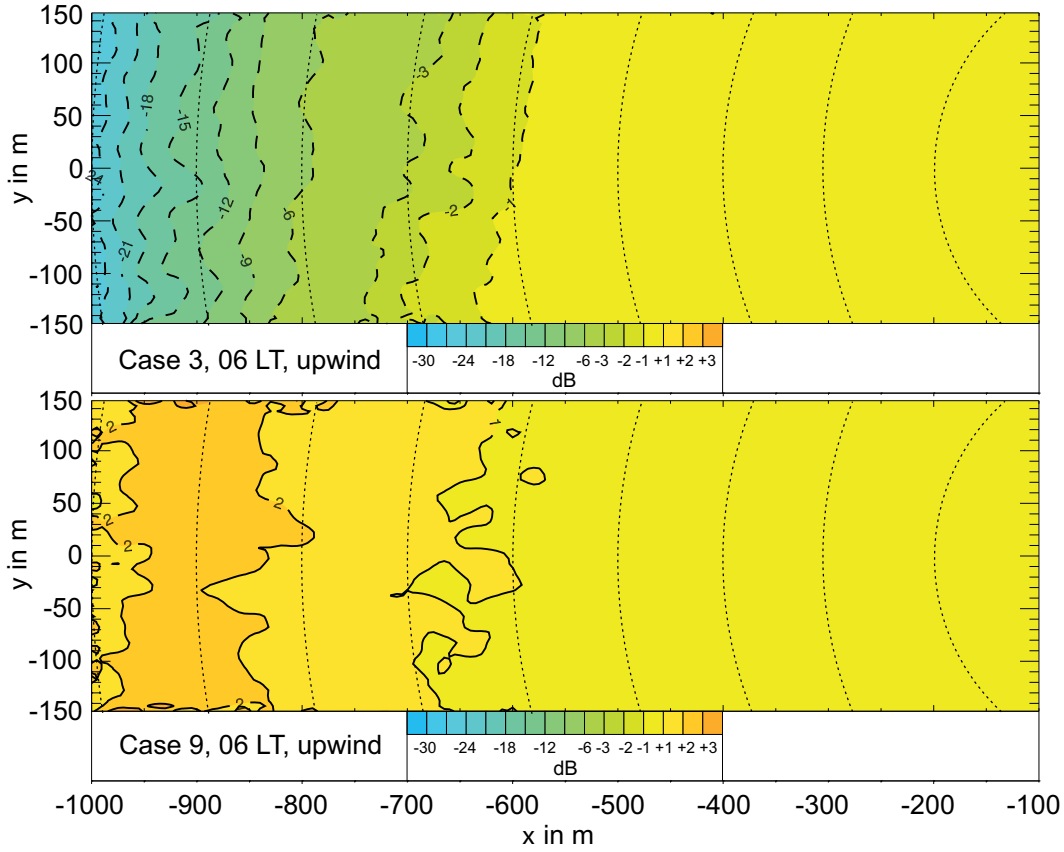

Figure 5: Near-ground (z_R = 2.5 m) relative sound level $L_A - L_{A,\mathrm{nr}}$ in the upwind domain. Top: Case 3, 06 LT, bottom: Case 9, 06 LT. The dotted lines are concentric around the wind turbine at $x = y = 0$ with an increment of 100 m.

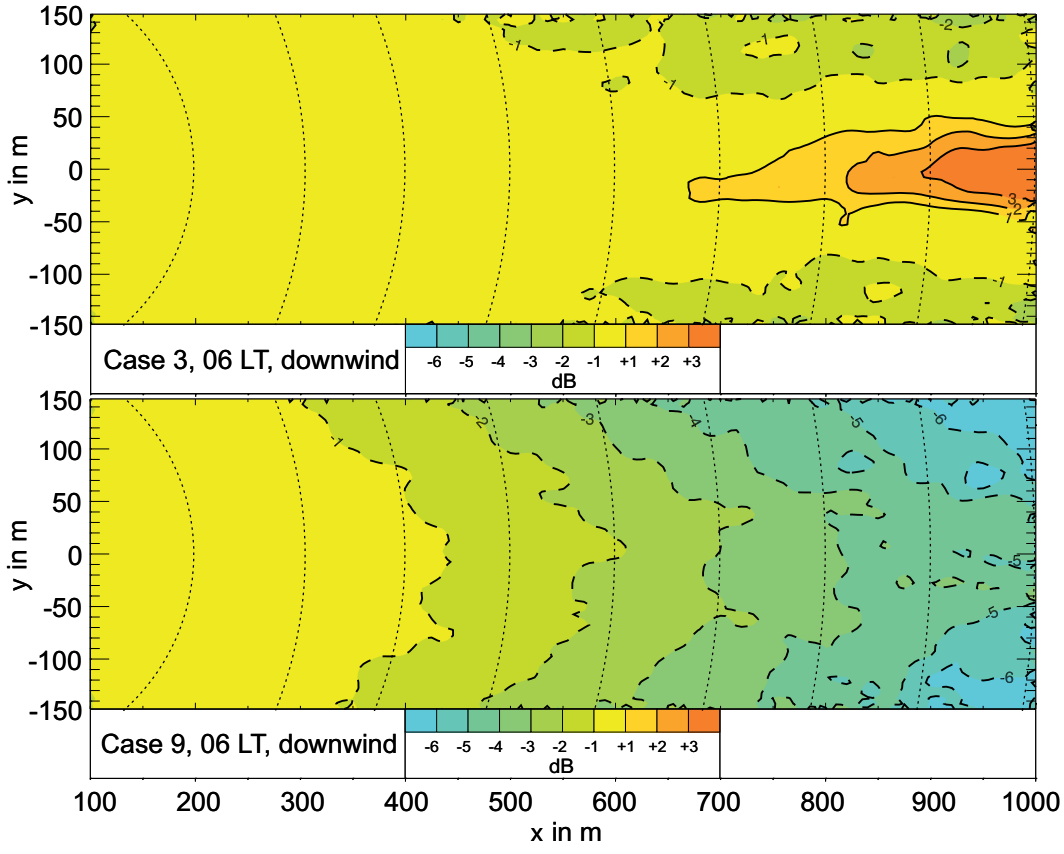

Figure 6: Same as Fig. 5, but for the downwind domain.

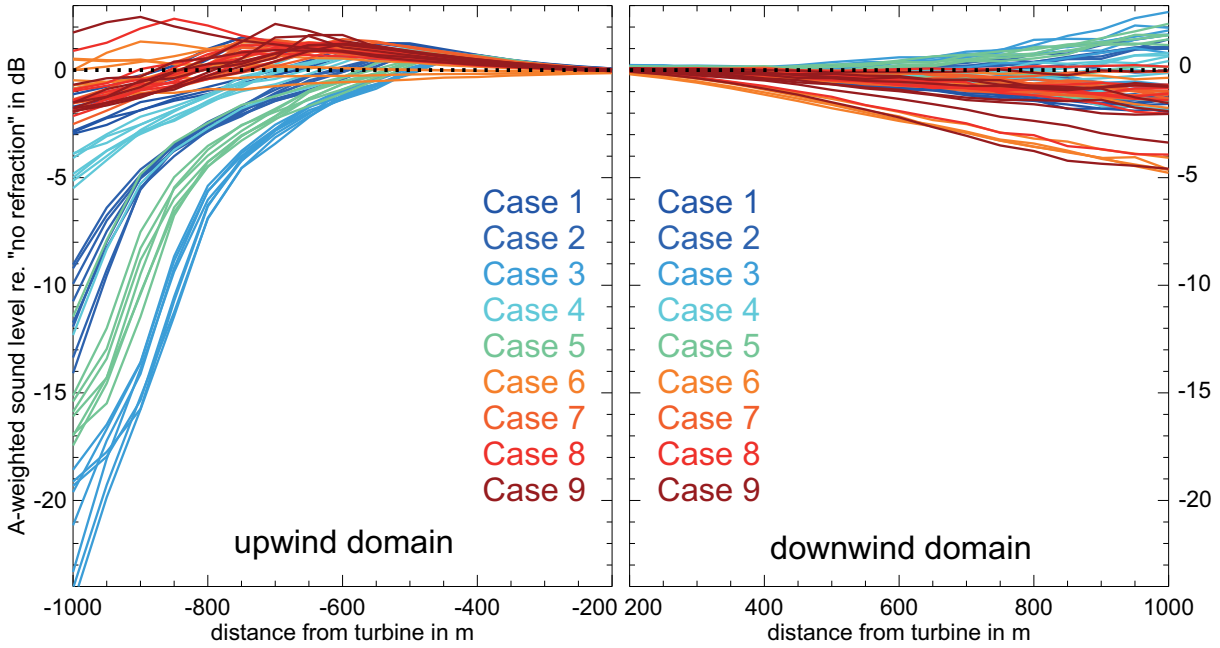

Figure 7: Horizontal profiles of the near-ground (z_R = 2.5 m) relative sound level $L_A - L_{A,\mathrm{nr}}$ for all cases (colours) and times of the day. The values are averaged between $y = -50$ m and $y = +50$ m. Left: upwind domain, right: downwind domain.

and downwind direction. The profiles are horizontally averaged within the stripe $-50\,\mathrm{m} \le y \le 50\,\mathrm{m}$ in order to get rid of local irregularities. The figure shows that the variability of the sound levels is much larger upstream of the turbine than it is downstream. At a distance of $|x| = 1000$ m refraction causes a variability of about 26 dB upstream, but only 8 dB downstream. The high variability in the upstream domain is caused by the varying position of the boundary of the acoustically shadowed far field which forms in most of the 72 situations as a consequence of upward refraction. The position of the shadow depends on the strength of refraction which varies with the situation. It also depends on the height of the source points. The shadow boundaries are not very sharp because sound from upper source points partly 'illuminates' the shadow zone belonging to lower source points. Turbulence also smooths the shadow boundary. In real outdoor situations, the sound-level variability in the far upwind domain is certainly smaller than 26 dB, because in the case of shadow forming ($L_A - L_{A,\mathrm{nr}} \ll 0$) the sound from the wind turbine is already very weak and likely to be masked by extraneous background noise. In addition, one has to note that the implemented model physics does not provide for scattering of (low-frequency) sound waves at turbulence which could add extra sound energy in the upwind shadow. The simulated sound levels in the refractive shadow are therefore mainly governed by refraction and diffraction. In Fig. 7 it is also apparent that the variability within the cases, i.e. the variability due to the diurnal cycle, is smaller than the variability from case to case, i.e. due to the changing large-scale meteorological background conditions.

The scatter plots in Fig. 8 illustrate how the effect of refraction on the sound level at 1000 m distance from the wind turbine depends on the background wind speed at hub level and the background static stability below hub level. The undisturbed background profile parameters were preferred to the turbine-modified parameters because they are more likely available either as measurements or weather-prediction model analyses. In the upwind domain at $x = -1000$ m the relative sound level $L_A - L_{A,\mathrm{nr}}$ is positive or weakly negative and almost independent of the stability for wind speeds at hub level below 5 m/s. Between 5 and 8 m/s $L_A - L_{A,\mathrm{nr}}$ is positive or weakly negative for stable stratification and strongly negative for unstable stratification. The situations with higher wind speeds are associated with near-neutral stratification and a shadow zone with strongly reduced sound levels. In the downwind domain at $x = +1000$ m the relative sound level is highest for neutral to isothermal stratification. Positive values of $L_A - L_{A,\mathrm{nr}}$ occur for high wind speeds of more than 6 m/s at hub level. The lowest values of $L_A - L_{A,\mathrm{nr}}$ are found for strongly stable stratification and wind speeds lower than 5 m/s.

A more distinct sorting of low and high relative sound levels at $|x| = 1000$ m results from the scatter diagrams of Fig. 9 where the mean vertical gradients of the unmodified background effective sound speed ($\partial\bar{c}_{\mathrm{eff},-x}/\partial z$ and $\partial\bar{c}_{\mathrm{eff},+x}/\partial z$, cf. Eq. 3.1) in the layer below the rotor $0 < z < z_{\mathrm{hub}} - r$ and in the rotor layer $z_{\mathrm{hub}} - r \le z \le z_{\mathrm{hub}} + r$ are the independent parameters. It turns out that the relative sound level is fairly well correlated with the mean vertical gradient of the effective sound speed in the rotor layer. This applies to the upwind as well as the downwind domain. The correlation

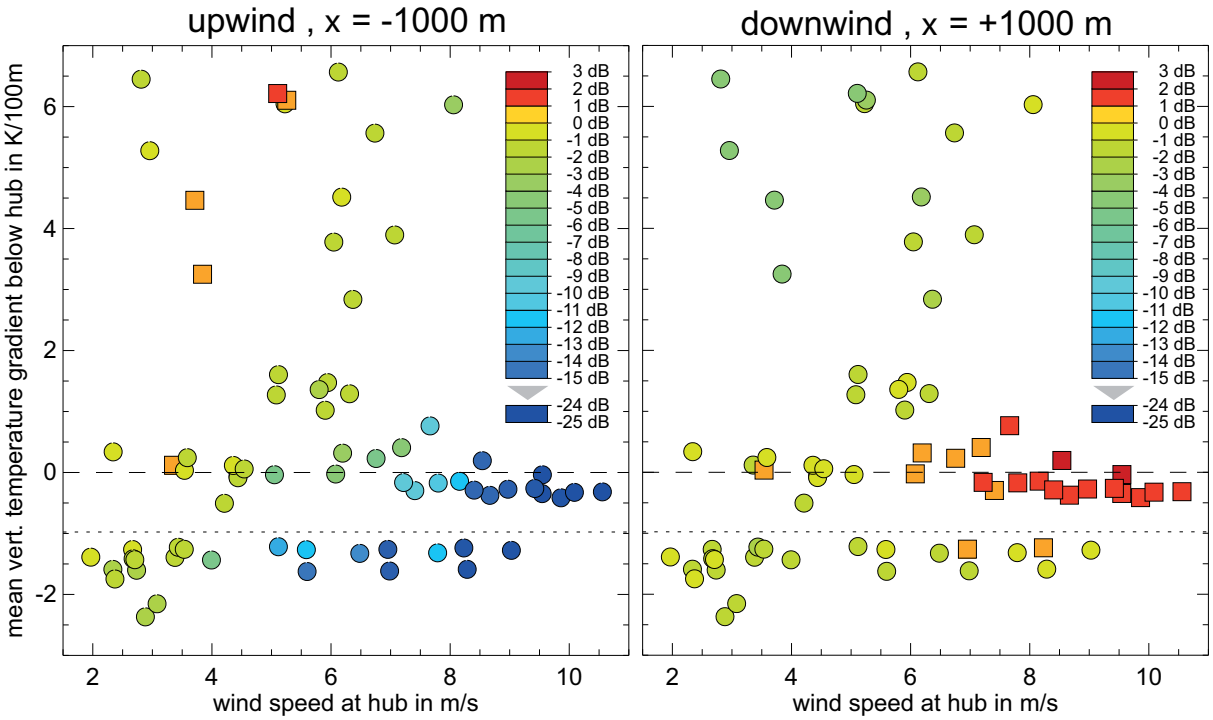

Figure 8: Near-ground (z_R = 2.5 m) relative sound level $L_A - L_{A,\mathrm{nr}}$ dependent on the wind speed at hub level (z = 100 m) and the mean vertical temperature gradient below the hub (z < 100 m). Left: upwind at $x = -1000$ m, right: downwind at $x = +1000$ m. Circles and squares signify negative and positive values of $L_A - L_{A,\mathrm{nr}}$, respectively.

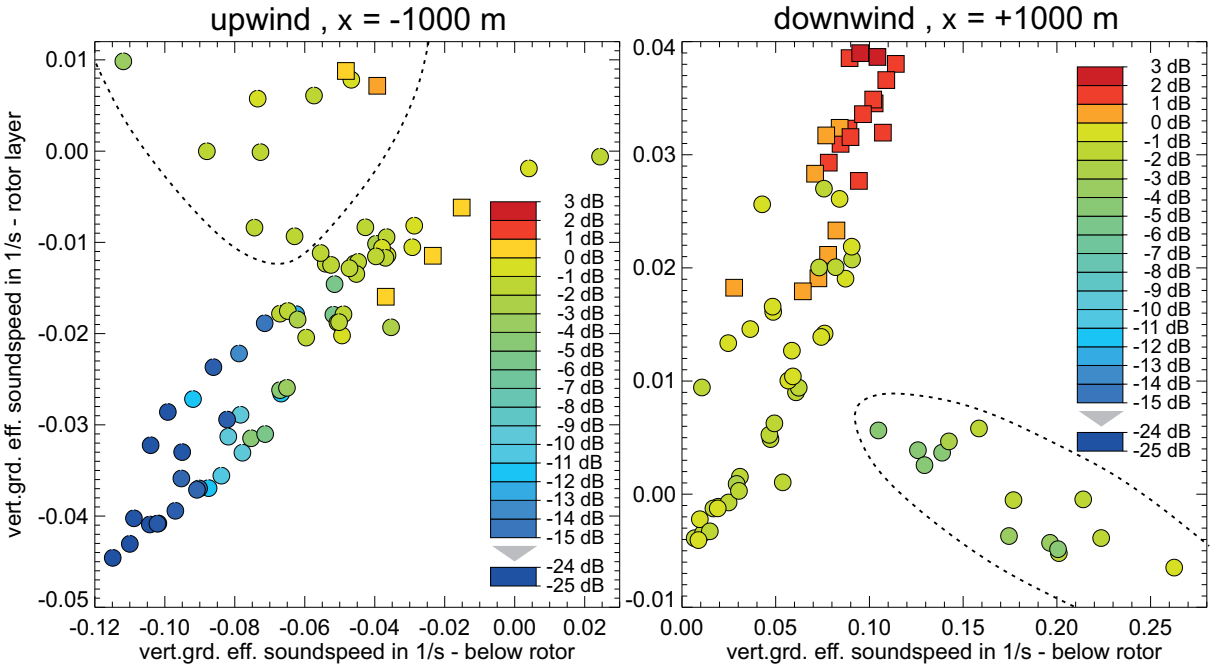

Figure 9: Near-ground (z_R = 2.5 m) relative sound level $L_A - L_{A,\mathrm{nr}}$ dependent on the vertical gradient of the effective speed of sound below the rotor (z < 50 m) and in the rotor layer (50 m ≤ z ≤ 150 m). Left: upwind at $x = -1000$ m, right: downwind at $x = +1000$ m. Circles and squares signify negative and positive values of $L_A - L_{A,\mathrm{nr}}$, respectively. Situations with uncorrelated effective sound speed gradients are enclosed by a broken line.

with the gradient in the layer below the rotor is worse. This is due to those situations which are enclosed by the broken lines in Fig. 9. In the upwind domain these situations (viz. Cases 1 and 9 at 21, 00, 03, and 06 LT) are associated with stable stratification and low-level jets, i.e. a strong wind speed increase with height below the hub level (z < z_{hub}) and only a weak wind speed increase or even decrease aloft. The relative sound levels of these situations are comparatively high. In the downwind domain this concerns the same situations and in

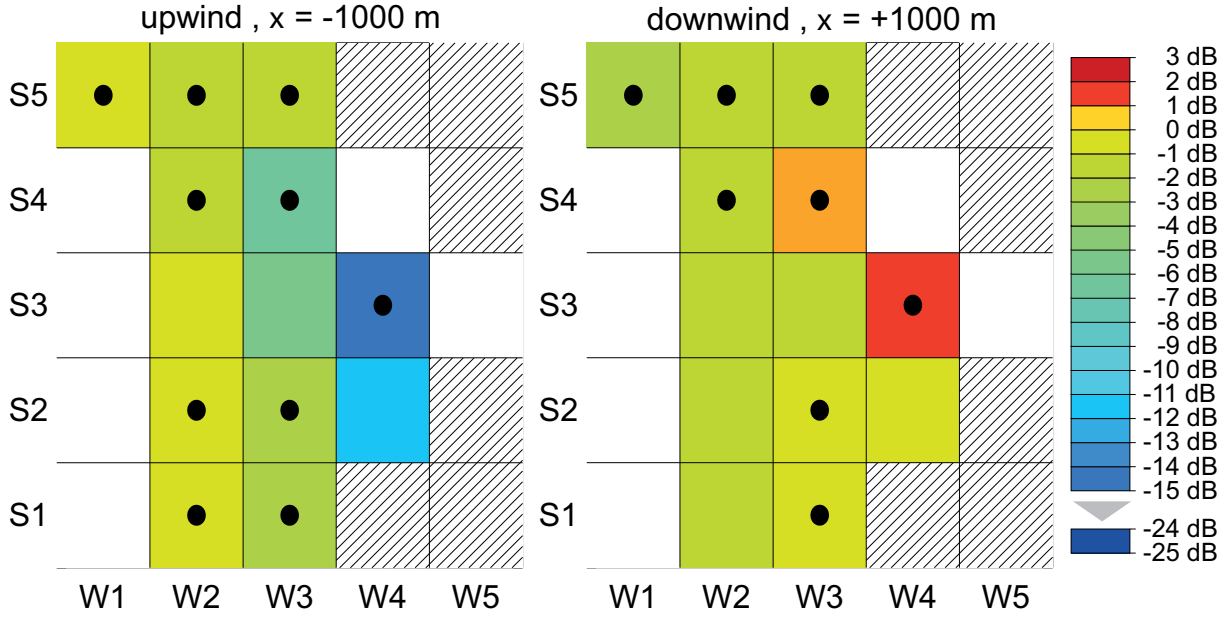

Figure 10: Class-specific average near-ground (z_R = 2.5 m) relative sound level $L_A - L_{A,\mathrm{nr}}$ of the Harmonoise classes. Left: upwind at $x = -1000$ m, right: downwind at $x = +1000$ m. Blank class combinations are not occupied by the 72 situations. Black dots denote significance (see text).

addition the nighty situations of Case 6. These situations are associated with the lowest relative sound levels at $x = +1000$ m On the other hand, positive values of $L_A - L_{A,\mathrm{nr}}$ (reddish squares in Fig. 9) are found at $x = -1000$ m for $-0.05\,\mathrm{s}^{-1} \le \partial\bar{c}_{\mathrm{eff},-x}/\partial z \le -0.01\,\mathrm{s}^{-1}$ in the layer below the rotor, and at $x = +1000$ m for $\partial\bar{c}_{\mathrm{eff},+x}/\partial z \ge 0.02\,\mathrm{s}^{-1}$ in the rotor layer.

The refraction effect on the sound level can also be allocated to meteorological classes. Classifications with a reasonable number of classes are beneficial because they facilitate the standardization of routine predictions. There are several classifications defined for air pollution predictions (e.g. Gifford, 1976; VDI 3783 Part 8, 2017). However, these classifications are of only limited suitability for sound propagation purposes as they do not discriminate between conditions for upward and downward refraction. A specific meteorological classification for noise predictions was proposed by Defrance et al. (2007), the so-called 'Harmonoise'-classification. This classification is based on five wind speed classes (W1-W5, increasing wind speed at 10 m above ground) and five stability classes (S1-S5, unstable to stable surface-layer stratification). The classification transfers the five wind speed classes by projection into nine classes of the wind speed component in the direction of propagation which is negative for upwind and positive for downwind propagation (V1-V9, strong upwind to strong downwind). Since the present study does not deal with cross-wind propagation, we use the wind speed classes W1-W5 and only distinguish between upwind and downwind propagation in the respective domains. Combinations of strong wind speeds (at 10 m above ground) and strongly unstable/stable stratification do not occur in the real atmosphere so that 19 W-S-class combinations remain.

Only 13 of the 19 possible combinations of classes are occupied by the 72 situations investigated in this study. The average relative sound level is shown in Fig. 10 for each of the occupied wind-stability class combinations in the upwind and downwind domain at $|x| = 1000$ m. Because the number of situations per class combination is unequally distributed and in some cases very small, not all class combinations are significant. The black dots in Fig. 10 indicate those class combinations which differ from at least one of the other combinations at a significance level of 0.05. Despite of the limited significance it turns out again that wind speed is dominating over stability in its influence on the effect of refraction on the near-ground sound level at 1000 m range. However, a reliable test of the applicability of the Harmonoise classification for the prediction of wind turbine noise would require a much larger database of different meteorological situations than presented here.

4 Discussion and conclusions

The sound propagation from a wind turbine was investigated with the help of coupled atmospheric and acoustical simulations. Eight instants of time during diurnal cycles for nine different large-scale cases resulted in 72 situations for which the boundary-layer profiles of wind and temperature, the wake flow, and the sound propagation from the wind turbine into upwind and downwind direction were calculated. Despite the rather large number of situations, the study does not by far cover the complete meteorological variety. Moreover, the study was restricted to one single turbine geometry (hub height, rotor diameter). Therefore, the acoustical results only show the meteorologically induced variability associated with the chosen conditions. More cases

and different dimensions of the turbine may lead to an even larger variability of sound levels.

The high number of situations required some limitations to keep the computational effort feasible. Contrary to recent studies (Barlas et al., 2017a,b; Heimann and Englberger, accepted) no large-eddy simulation (LES) model was used but a Reynolds-averaged Navier-Stoke (RANS) model. Moreover, the domain size was limited to a maximum range of $|x| = 1000$ m. Nevertheless, unlike the simulations by Heimann et al. (2011), Barlas et al. (2017a), Heimann et al. (2018) or Heimann and Englberger (accepted) also the upwind domain was considered.

The results show that the meteorological variability leads to refraction-induced variations of the near-ground sound level which increase with range. This applies to both domains, upwind and downwind, with the meteorologically induced variability being larger on the upwind side, at least within the 1000 m range limit. The strongest reduction of the sound level in the upwind domain is associated with strong wind speeds which cause acoustical shadowing for $x < -700$ m. Vice versa, strong winds increase the sound level below the wake in the downwind domain. The results of Barlas et al. (2017a,b) and Heimann and Englberger (accepted) suggest, that there is an even stronger enhancement beyond $x > +1000$ m and that this enhancement is not only caused by a high wind speed, but also by stable stratification and the corresponding intensity and extent of the wind speed deficit in the wake. This could not be systematically investigated in the present study because of the range limitation. However, it has to be noted that in the far field the absolute sound levels are already relatively low due to geometrical spreading. Hence, they are likely to be masked by the background noise level.

For practical reasons it would be profitable to find a meteorological classification scheme which is applicable to wind turbine noise predictions. Such a scheme should have as few classes as possible, and the classes should differ in terms of sound level, i.e. the class definitions must be relevant to sound propagation effects. The Harmonoise classification, which was designed for road and rail noise, i.e. near-ground sources, does not seem to be the best choice for wind turbine noise. Aside from the fact that too few situations were available for a robust evaluation, many classes differ only slightly with respect to the sound level. In particular, it is questionable whether a class definition that is based on surface-layer parameters is able to discriminate between acoustically different situations for propagation from elevated sources. The sound propagation from a wind turbine is much more influenced by parameters in the rotor layer, the wind-turbine wake and the existence of a low-level jet rather than by near-surface parameters.

The present study is a step towards a comprehensive survey of the meteorological impact on the sound levels around a wind turbine. The full climatic variety of meteorological situations has to be represented by a much higher number of cases than in this study. A range of up to 2 km should be considered as well as oblique and cross-wind propagation. Of course, the geometry of the turbine (hub height, rotor diameter) should also be varied as it determines the ray paths and thus the refraction regimes that are passed during propagation. The same applies to topographical features (forests, hills) around the turbine and the influence of neighbouring turbines in wind parks. Because the number of parameters and the degree of freedom can be rather high, generic approaches to describe the meteorological influence on wind turbine sound propagation cannot fully substitute individual simulations of specific configurations of turbine and topography.

Acknowledgement

This research was performed as part of the LIPS project, funded by the German Federal Ministry for Economic Affairs and Energy under grant no. 0325518 by a resolution of the German Federal Parliament.

References

Barlas, E., W.J. Zhu, W.Z. Shen, M. Kelly, S.J. Andersen, 2017a: Effects of wind turbine wake on atmospheric sound propagation. – Appl. Acoust. **122**, 51–61. DOI: 10.1016/j.apacoust.2017.02.010.

Barlas, E., W.J. Zhu, W.Z. Shen, K.O. Dag, P. Moriarty, 2017b: Consistent modelling of wind turbine noise propagation from source to receiver. - J. Acoust. Soc. Amer. **142**, 3297–3310. DOI:10.1121/1.5012747.

Bingöl, F., J. Mann, G.C. Larsen, 2010. Light detection and ranging measurements of wake dynamics. Part I: one-dimensional scanning. – Wind Energy **13**, 51–61. DOI: 10.1002/we.352.

Bowdler, R., G. Leventhall, 2012: Wind Turbine Noise. – Multi-Science Publishing Co. Ltd, ISBN 978-1-907132-30-8.

Defrance, J., E. Salomons, I. Noordhoek, D. Heimann, B. Plovsing, G. Watts, H. Jonasson, X. Zhang, E. Premat, I. Schmich, F. Aballea, M. Baulac, F. de Roo, 2007: Outdoor Sound Propagation Reference Model Developed in the European Harmonoise Project. – Acta Acustica united with Acustica **93**, 213–227.

Delany, M.E., E.N. Bazley, 1970. Acoustical properties of fibrous absorbent materials. – Appl. Acoust. **3**, 105–116.

Dyer, A.J., 1974. A review of flux-profile relationships. – Bound.-Layer Meteor. **7**, 363–372.

Deutsche WindGuard, 2015: Schallemissionsmessungen an einer Windenergieanlage. – Bericht MN15016.A1, 49 pp.

Englberger, A., A. Dörnbrack, 2017. Impact of the diurnal cycle of the atmospheric boundary layer on wind-turbine wakes: A numerical modelling study. – Bound.-Layer Meteor., published online. DOI:10.1007/s10546-017-0309-3.

Gifford, F.A., 1976: Turbulent diffusion typing schemes: a review. – Nuclear Safety **17**, 68–86.

Goedecke, G.H., H.J. Auvermann, 1997: Acoustic scattering by atmospheric turbules. – J. Acoust. Soc. Amer. **102**, 759–771. DOI:10.1121/1.419951.

Gross, G., 2010: Numerical simulations to the diurnal variation of wakes behind wind turbines. – Meteorol. Z. **19**, 91–99. DOI:10.1127/0941-2948/2010/0418.

Hansen, K.S., R.J. Barthelmie, L.E. Jensen, A. Sommer, 2012: The impact of turbulence intensity and atmospheric stability on power deficits due to wind turbine wakes at Horns Rev wind farm. – Wind Energy **15**, 183–196. DOI: 10.1002/we.512.

Heimann, D., R. Blumrich, 2004: Time-domain simulations of sound propagation through screen-induced turbulence. – Appl. Acoust. **65**, 561–582. DOI:10.1016/j.apacoust.2003.09.007.

Heimann, D., A. Englberger, 2018: 3D-simulation of sound propagation through the wake of a wind turbine: impact of the diurnal cycle. – Applied Acoustics. DOI:10.1016/j.apacoust.2018.06.005.

Heimann, D., G. Gross, 1999: Coupled simulation of meteorological parameters and sound intensity in a narrow valley. – Appl. Acoust. **56**, 73–100.

Heimann, D., Y. Käsler, G. Gross, 2011: The wake of a wind turbine and its influence on sound propagation. – Meteorol. Z. **20**, 449–460. DOI:10.1127/0941-2948/2011/0273.

Heimann, D., A. Englberger, A. Schady, 2018: Sound propagation through the wake flow of a hill-top wind turbine – a numerical study. – Wind Energy **21**, 650–662. DOI:10.1002/we.2185.

ISO 9613-1, 1993: Acoustics; attenuation of sound during propagation outdoors; part 1: calculation of the absorption of sound by the atmosphere. – Available from the International Organization for Standardization – www.iso.org.

Larsson, C., O. Öhlund, 2014: Amplitude modulation of sound from wind turbines under various meteorological conditions. – J. Acoust. Soc. Amer. **135**, 67–73. DOI:10.1121/1.4836135.

Lee, S., D. Lee, S. Honhoff, 2016: Prediction of far-field wind turbine noise propagation with parabolic equation. – J. Acoust. Soc. Amer. **140**, 767–778. DOI:10.1121/1.4958996.

Mellor, G.L., T. Yamada, 1974: A hierarchy of turbulence closure models for planetary boundary layers. – J. Atmos. Sci. **31**, 1791–1806. DOI:10.1175/1520-0469.

Öhlund, O., C. Larsson, 2015: Meteorological effects on wind turbine sound propagation. - Appl. Acoust. **89**, 34–41. DOI: 10.1016/j.apacoust.2014.09.009.

Paulson, A., 1970: The mathematical representation of wind speed and temperature profiles in the unstable atmospheric surface layer. – J. Appl. Meteor. **9**, 857–861.

Pielke, R.A., 1984: Mesoscale Meteorological Modeling. – Academic Press, Orlando. ISBN: 9780080491820.

Pierce, A.D. 1981: Acoustics – An introduction to its physical principles and applications. – McGraw-Hill Inc., New York, 619 pp.

VDI 3783, Part 8, 2017: Environmental meteorology: Turbulence parameters for dispersion models supported by measurement data, – Beuth-Verlag, Berlin.